Proceedings of ASME Turbo Expo 2011
GT2011
June 6-10, 2011, Vancouver, British Columbia, Canada

GT2011-46126

STATISTICAL EVALUATION OF CFD PREDICTIONS OF MEASURED MIXING PROPERTIES OF HYDROGEN AND METHANE FOR LEAN PREMIXED COMBUSTION

Amin Akbari, Scott Hill, Vincent McDonell, and Scott Samuelsen
UCI Combustion Laboratory
University of California
Irvine, CA 92697-3550 USA

ABSTRACT

Hydrogen is a fuel of interest to the combustion community research as a promising sustainable alternative fuel to replace fossil fuels. The combustion of hydrogen produces only emission of water vapor and NO_x. To alleviate the NO_x emission, lean combustion has been proposed and utilized in last three decades for natural gas. Therefore, evaluation of mixing properties of both methane and hydrogen in lean combustion technology such as premixers is crucial for design purposes. Increased capability of computational systems has allowed tools such as computational fluid dynamics to be regularly used for purpose of design screening. In the present work, systematic evaluation of different CFD approaches is accomplished for axial injection of fuel into non swirling air. The study has been undertaken for both methane and hydrogen. Different Reynolds Averaged Navier Stokes (RANS) turbulence models including $k-\varepsilon$ and RSM, which are relatively attractive as being computationally efficient, are evaluated. Further, the sensitivity of RANS models to different turbulent Schmidt number (Sc_t), as an important parameter in mass transport analysis, has been investigated. To evaluate the numerical results, fuel concentration is measured in different locations downstream of the injection point. This is accomplished by means of flame ionization detector (FID). Finally, a comprehensive comparison has been made between numerical and experimental results to identify the best numerical approach. To provide quantitative assessment, the simulations follow a statistically design matrix which allows analysis of variance to be used to identify the preferred simulation strategies. The results suggest high sensitivity of numerical results to different Sc_t and relatively low sensitivity to turbulence models. However, this general trend is the opposite for radial fuel injection.

NOMENCLATURE

A	physical area
C_d	discharge coefficient
D	diameter
k	turbulent kinetic energy
$\dot{m}$	mass flow rate
P	pressure
R	specific gas constant
$Sc_{,t}$	turbulent Schmidt number
T	temperature
U	velocity
X,Y,Z	coordinate
ε	dissipation rate
ρ	density

Subscripts

fuel	fuel
jet	jet
bulk	air

INTRODUCTION

Finding alternative fuels for power generation systems is a priority for energy research in the 21st century as interest in reducing greenhouse gases (GHGs) [1]. Hydrogen, if produced from appropriate renewable feedstocks and processes, is one candidate for the replacement of the current carbon-based energy services and can greatly reduce the emissions of GHGs [2]. The combustion of hydrogen precludes emission of CO_2, CO, SO_2, VOCs and particles, hence the only major species produced is water and the only major pollutant of concern is NO_x [3,4,5]. For gas turbine applications, a key driver for technology development is low NOx emissions. To achieve low NO_x emissions, it is important to avoid high temperatures

which form "thermal NOx". A strategy which has been widely implemented in advanced natural gas fired gas turbines is lean premixed combustion. As a result of the experience gained through development of ultra low emissions natural gas fired turbines, it is desirable to apply this knowledge and understanding to alternative fuels such as hydrogen. However, the use of hydrogen poses challenges for the design of a system due to (1) the high laminar flame speed of hydrogen compare to natural gas that can contribute to flashback in the combustor; and (2) the wide flammability range of hydrogen. Hence, appropriate premixer designs to prepare the fuel/air mixture before it enters the combustor are critical to overcome these challenges while producing an appropriate mixture to achieve low NOx emissions. Consequently, additional attention to the premixer is warranted. Due to the great practical importance of mixing, several methods such as numerical, analytical and experimental analyses have been used to study and predict this phenomenon. Since simple analytical approaches are generally not able to provide accurate information in broad range of various configurations, computational fluid dynamics (CFD) modeling can be utilized as a design tool for the assessment of relevant parameters of the investigated system [6]. The use of CFD as a design tool for fairly complex geometries has been made possible in recent years as a result of enhanced computer power. What is not clear is the relative accuracy of these methods.

In terms of fuel/air mixing, different fuel injection strategies can be considered. In gas turbine premixers fuel may be injected radially to the main flow or along the axis. In many practical configurations, fuel injected from (1) the tip of a centerbody as a "pilot" and (2) radially into a crossflowing air stream. The pilot reaction is used to help stabilize the lean reaction produced by radial injection and to tune out combustion oscillations. Previously, the behavior of the radially injected fuel was considered [7]. In the present work, the behavior of this axial injected "pilot" fuel is considered. Further, as a starting point, non-swirling flow is considered to compliment the previous radial jet study [7]. Non-swirling axisymmetric flows form a significant class of turbulent flows in combustion applications [8]. The flow structure of free round turbulent jets has been widely studied in last three decades, and several analytical and numerical approaches have been suggested to resolve the fluctuation of properties these flows [9,10,11,12,13]. Most numerical work carried out for free round jets have considered simple geometries, such as cubical or cylindrical domains entailing a round jet injected from a nozzle. Few studies have considered complex geometries that resemble practical systems. In the present work, mixing of fuel in a complex 3D premixer configuration that entails non-swirl axial injection of fuel into air co-flow has been studied.

Simulations are carried out for both methane and hydrogen in an axial injection configuration to assess the relative accuracy of different CFD modeling strategies. Reynolds Stress and k-epsilon turbulence models are used with Reynolds Average Navier-Stokes (RANS) simulations as the typical approach in current industrial design practice. Moreover, the sensitivity of CFD results to variation of different turbulent Schmidt numbers (Sc_t) is studied. Sc_t is an important parameter in mass transfer equations that must be defined properly in numerical studies to establish a robust numerical strategy. By definition, Sc_t is the ratio of turbulent molecular kinematic viscosity and turbulent mass diffusivity which estimates the mixing behavior in turbulent flows. The appropriate reported Sc_t for RANS models depends on the local flow characteristics [14]. Thus, in this work four different Sc_t numbers varying from 0.2 to 0.7 are tested.

The objective of this work is to evaluate the capabilities of different CFD modeling approaches to obtain reliable predictions of mixing properties of methane and hydrogen in axial injection configuration of a 3D complex premixer. The capability of the CFD strategies are assessed by comparison with experimental studies carried out in parallel.

NUMERICAL AND EXPERIMENTAL METHODS

Numerical Methods

Computational fluid dynamics (CFD) modeling is widely used in industrial design practices. A wide range of computational time is required depending on the approach taken. Direct numerical simulation (DNS) can, in principle, provide the most accurate information about turbulent flows; however the computational facilities and expertise costs required for conducting DNS for most practical gas turbine applications make it unfeasible in the near term. Large eddy simulation (LES), with less associated costs, has been developing to capture some of the benefits of DNS, yet still be applicable to practical applications. Nonetheless, the computational costs for LES for industrial designs are still high [15]. Thus, Reynolds averaged Navier-Stokes (RANS) turbulence models continue to be relied upon in industry in the near term for design. This approach reduces the computational efforts significantly by averaging the governing equations over time. A detailed discussion about the details of RANS models is provided in turbulent classical text books [16]. Of the turbulence models used in RANS, the $k-\varepsilon$ model, using the Boussinesq hypothesis is the most common. This model requires relatively low computational cost. The main disadvantage of this model is the assumption of isotropic scalar quantities for the flow field which is not always true for the real flows [16]. The Reynolds stress turbulence model (RSM) relaxes the isotropic turbulence assumption of the $k-\varepsilon$ model by providing five additional governing equations which in principle can provide more accurate flow field behavior [16].

In the present work, the sensitivity of numerical results to different turbulence models is evaluated. In addition, to study mass transport variation due to different turbulent Schmidt numbers (Sc_t), four different Sc_t are examined.

Grid and Numerical scheme

Generation of a high quality grid for the geometry which is being studied is critical. In the present work, grid generation is accomplished in Gambit. For simple 2-D and 3-D geometries, a structured grid is commonly used due to its

stability and simplicity [17]. However, for complex 3-D geometries with sharp edges and a wide range of physical dimensions, structured grid generation is quite challenging and inflexible. As a result, for the present work, an unstructured grid is generated for the domain including tetrahedral mesh elements. This allows flexibility to use very fine grid cells near the injection point to capture rapid flow field scalar variation near this point. Studies have shown that appropriate unstructured grids give results that are consistent with structured grid, though more grid points generally result with an unstructured approach [17]. In the present work, grid sensitivity studies are carried out to ensure grid quality. It is apparent that, in the present case, symmetry can potentially be taken advantage of to reduce the computational time. Hence grids were generated for both quadrant and full body geometries. This is explored in the present work. The details of grid generation can be seen in Figure 1.

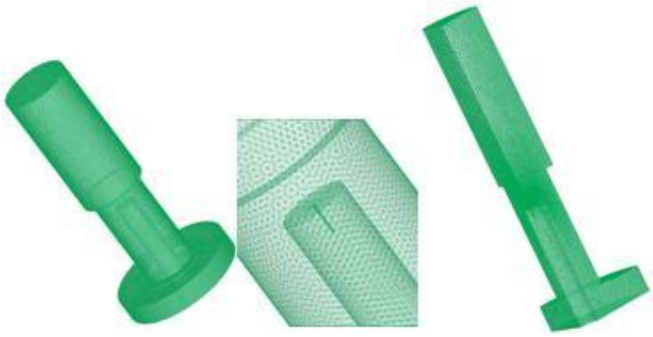

Figure 1-details about grid generation: entire domain, near injection refinement, and quadrant body grid, from right to left of the figure.

The computational work was carried out on an 8 node Beowulf cluster each with 4 GB RAM. AMD Opteron 2.6GHz CPUs, with 1MB cache, were used. The operating system is Redhat 4 64 bit OS Advance Server and the nodes are connected via a GigE Nortel switch.

Experiment

The experimental set up is shown in Figure 2. Air enters the air plenum through four tangential ports. To remove residual swirl, a sintered copper ring and a metal honeycomb flow straightener are placed in the rig. An axial injection cap with a single hole with diameter of 1.1938 mm is installed on the centerbody to provide the axial fuel injection. A straight quarl module is used with an 80 mm i.d. quartz liner.

The fuel mass flows were controlled by a mass flow controller (Brooks Instruments 5851i mass flow controller and 0154 read out and control unit). The air flow is metered by a sonic venturi calibrated with a NIST traceable laminar flow element and controlled with a precision metering valve.

Fuel concentration is measured at three planes downstream of the injection point as shown in Figure 3 as well as along the centerline. Samples of the gas are gathered using an extractive probe (3.175 mm diameter) and analyzed using a gas chromatograph (Agilent). A vacuum pump was to pull a small sample of the flow for analysis.

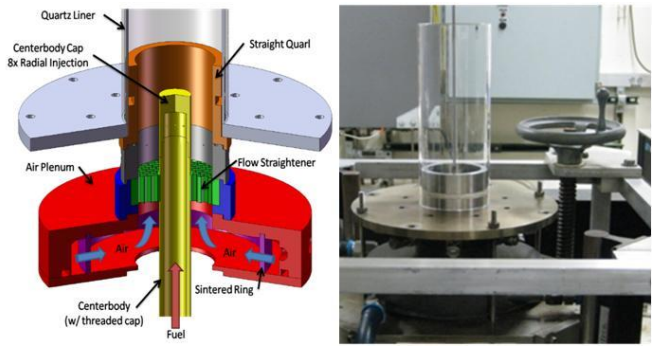

Figure 2-schematic components of experimental hardware versus to real picture of experimental set up.

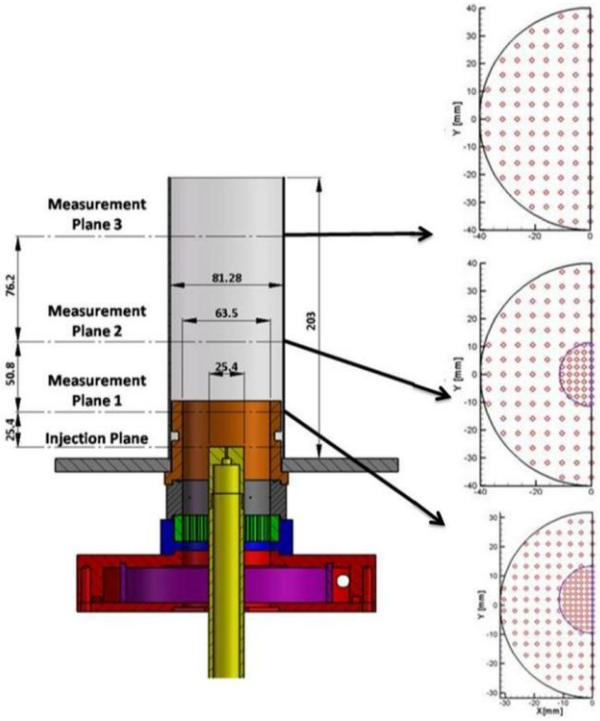

Figure 3-premixer cross section, and measurements planes.

The sample probe was positioned to within 0.0127 mm by moving the premixer assembly via a three axis worm gear system. The spatial position is monitored using a precision glass rule and an optical pickup (Mitutoyo). A settling time of 30 seconds was used between any movement of the location of the premixer and measurement initiation. Isokinetic conditions could not be fully established at all locations. However the probe flow rate was varied by a factor of 2.5 at several locations in the measurement domain and found to vary by less than 10%.

Due to the symmetric nature of the flow field, time-averaged measurements are taken in half of each plane. At each location, multiple readings were obtained over a 6 minute period. As shown in Figure 3, the resolution of sample measurements was adapted to capture the details of gradients in fuel concentration near the centerline.

Boundary Conditions

To conduct a meaningful comparison between numerical and experimental results, the imposed boundary conditions must match the physical conditions. The fuel and air mass flow rates are matched for both numerical and experimental studies. No mass is recirculated through the exit plane which discharges to the atmosphere. As a result, the outlet boundary is set to atmospheric pressure. Due to the fluid mechanics within the fuel injection hole, this inlet condition must be treated with care. The discharge coefficient of this hole will have an impact on the velocity of the fuel. In the present work, the following correlation was used [18, 19]:

$$C_d = \frac{\dot{m}_{fuel}}{A_{jet}} \sqrt{\frac{R_{fuel} T_F}{2 P_{Bulk} (P_{Fuel} - P_{Bulk})}} \qquad (1)$$

In the present work, the same flowrates of methane and hydrogen used for a similar study featuring radial injection of the fuel into the air were used [7]. A momentum flux ratio of ~9 was used for the two fuels arrived via Equation 2:

$$J = (\rho_j U_j^2)/(\rho_b U_b^2) \qquad (2)$$

The resulting conditions studied are shown in Table 1.

Table 1-boundary conditions for the current study.

Quarl Module	Straight Barrel, No Contraction	
Flow Swirl	None, Flow Straightener Used	
Bulk Flow Rate [kg/s]	0.0186	
Jet Area [m^2]	0.00000112	
Injection Type and #	Axial, 1x	
Injection Height	At top of quarl	
Case	H_2 into Air	CH_4 into Air
H_2 Mass Flow per hole [kg/s]	6.15×10^{-6}	-
CH_4 Mass flow per hole [kg/s]	-	1.8×10^{-5}
Fuel Specific Gas Constant[J/k mol]	8314.47	518.26
Momentum Flux Ratio	8.9	9.5
Pressure Difference [Pa]	358.4	353.4
Bulk Pressure [kPa]	101.7	101.7
Fuel Temperature [k]	294.3	294.3
Coefficient of discharge C_d	.658	.742
no-slip wall condition is used for all of numerical cases		

RESULTS AND DISCUSSION

In this section, three types of results are presented. First, examples of the sensitivity to geometry are shown along with grid sensitivity. This is followed by comparison of the experimental and numerical results. This comparison is presented in two forms: contours and radial/centerline profiles. Finally, a statistical analysis is carried out to more quantitatively assess the results.

Geometry and Grid Sensitivity

In an effort to more efficiently execute the numerical simulation matrix, consideration was given to use of a quarter sector of the geometry with periodic boundaries. This study reveals serious shortcomings in the quarter sector approach. For example, qualitative comparison between quadrant body and full geometry case with experimental measurement is shown in Figure 4 .

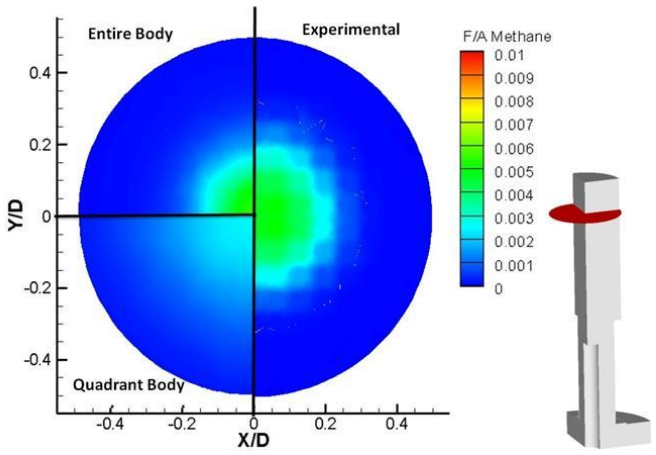

Figure 4-quadrant body and entire body vs experimental measurement at Z/D=1.875.

It is apparent that the quarter section overpredicts the level of mixing at this plane and that the results from the full geometry present better agreement with measured values. In order to get more quantitative sense of this comparison, a diametric profile of the fuel to air ratio is shown in Figure 5. As shown, the full geometry provides a closer match to the experimental results. As a result of this evaluation, the entire geometry was used for the balance of the simulation work.

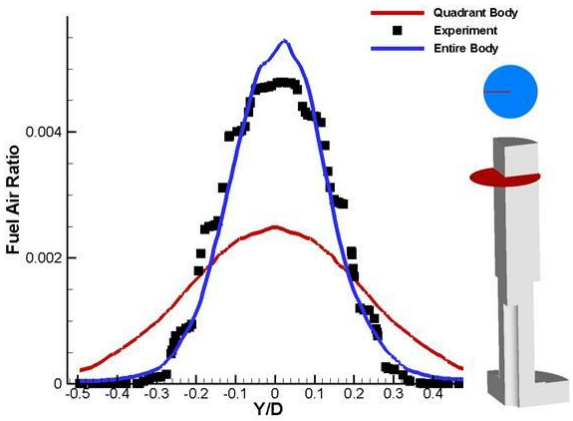

Figure 5-radial distribution of fuel air ratio for quadrant body vs entire body at Z/D=1.875.

To ensure grid independence, sensitivity of the solutions to grid structure was carried out. The grids considered included super coarsened, coarsened, intermediate, refined and super

refined cases with approximately 200×10^3, 300×10^3, 500×10^3, 600×10^3, and 1400×10^3 cells, respectively. All of the grids were examined for different fuels and turbulence models to establish the grid for use in the detailed comparison studies. For each case, it was confirmed that further refinement did not result in significant change in the numerical solution of the fuel to air ratio throughout the domain. The summary of final cell counts for each case is given in Table 2.

Table 2-Numerical cases in this work for 3D axial injection non-swirl configuration.

Turbulence Model	Fuel	Oxidant	Sc_t	# of Grid
$k-\varepsilon$	Methane	Air	0.2	287×10^3
$k-\varepsilon$	Methane	Air	0.3	287×10^3
$k-\varepsilon$	Methane	Air	0.4	287×10^3
$k-\varepsilon$	Methane	Air	0.7	287×10^3
RSM	Methane	Air	0.2	539×10^3
RSM	Methane	Air	0.3	539×10^3
RSM	Methane	Air	0.4	539×10^3
RSM	Methane	Air	0.7	539×10^3
$k-\varepsilon$	Hydrogen	Air	0.2	287×10^3
$k-\varepsilon$	Hydrogen	Air	0.3	287×10^3
$k-\varepsilon$	Hydrogen	Air	0.4	287×10^3
$k-\varepsilon$	Hydrogen	Air	0.7	287×10^3
RSM	Hydrogen	Air	0.2	625×10^3
RSM	Hydrogen	Air	0.3	625×10^3
RSM	Hydrogen	Air	0.4	625×10^3
RSM	Hydrogen	Air	0.7	625×10^3

Methane

Comparative results for methane injected into air are now presented. An overall view of fuel dispersion in the X-Z plane is presented in Figure 6 for $k-\varepsilon$ and RSM turbulent models. The overall predicted fuel distribution for both numerical models are similar. However, the predicted level of mixing using $k-\varepsilon$ appears slightly faster than when using RSM.

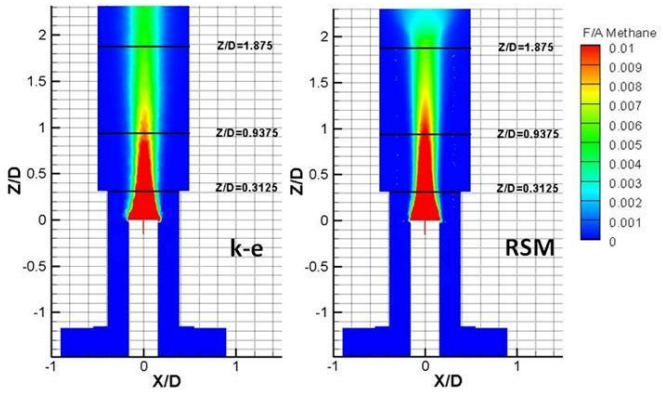

Figure 6- Contours of methane fuel to air in the plane of Y/D=0 for $k-\varepsilon$ and RSM simulations

Figure 7 presents the methane mole fraction distribution along the centerline from the injection point to the exit of the premixer and underscores the fast mixing achieved. It is apparent that mole fraction of methane undergoes a sharp change near the injection point which may cause challenges both experimentally as well as in comparing results at specific planes. Recall that the laminar Sc for methane and air is 0.99. However the typical value for Sc_t is generally 0.7 [17]. In the current application, it is likely that turbulent mixing dictates the fuel distribution more than does the laminar mass diffusion.

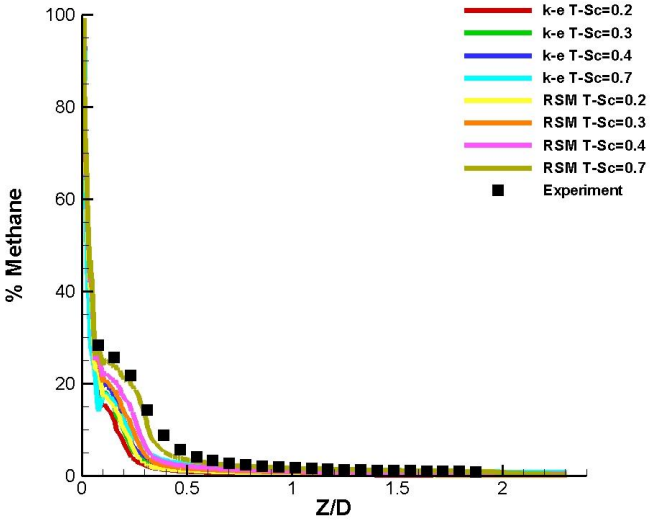

Figure 7- centerline traverse comparison for all of the methane cases at X=Y=0.

It is clear that the RSM model with Sc_t=0.7 results in the best agreement with measured values. It is also evident that large gradients in the fuel concentration occur in the Z direction, indicating the importance of carefully matching the measurement and simulation locations when comparing results.

A comparison of the measured and predicted fuel air ratio results is now discussed for the three axial planes. The first plane is located 25.4 mm downstream of injection point or Z/D=0.3125. The radial distribution of results is given in Figure 8. The schematic indicates the location of this plane in the current geometry. It is apparent that, except for RSM with Sc_t=0.7, the agreement between predicted and measured results is generally poor. Note that this location is in the region of steep concentration gradients along the centerline; hence some of the variation noted may be due to positioning accuracy.

For both RANS turbulence models the predicted results approach the experimental data as Sc_t increases. To investigate the sensitivity of predicted results to different Sc_t numbers, Figure 9 presents the contour of methane to air ratio for both turbulence models and for different values of Sc_t.

The relatively weak overall agreement of simulations with the measured values at this plane can be attributed to (1) the flow separation near the injection cap which makes the flow field dynamic and (2) the high gradients in this part of the as shown in Figure 7.

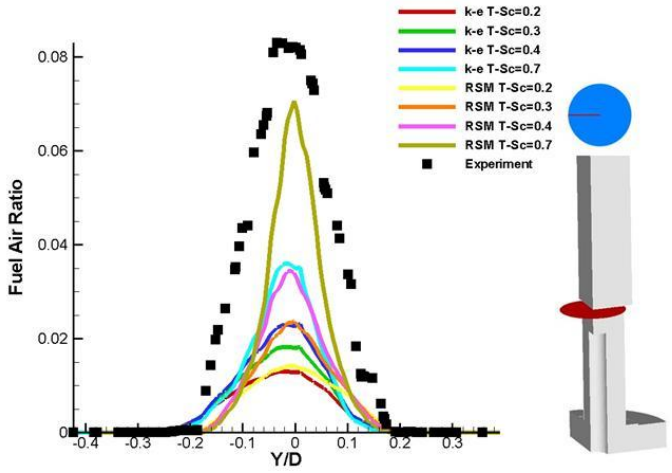

Figure 8- Comparison of measured and predicted methane to air ratio at Z/D=0.3125.

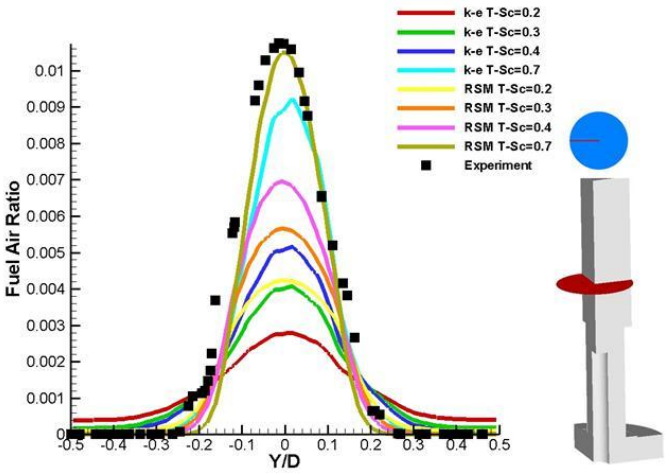

Figure 10- Comparison of measured and predicted methane to air ratio at Z/D=0.9375.

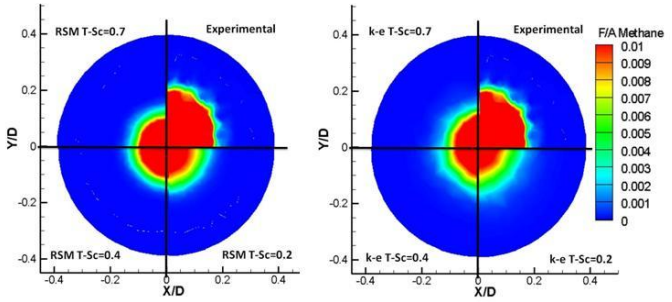

Figure 9-sensitivity of $k-\varepsilon$ and RSM methane to air ratio predictions to various Sc_t at Z/D=0.3125.

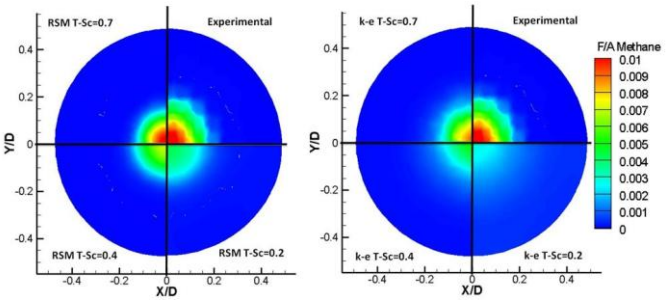

Figure 11- sensitivity of $k-\varepsilon$ and RSM methane to air ratio predictions to various Sc_t at Z/D=0.9375.

The second plane is located at Z/D=0.9375. In this plane the jet of fuel has more time to mix with the co-flowing air. Radial profiles are shown for numerical cases and experimental measurements in Figure 10.

Similar to the first plane, a wide range of simulations results are observed. However, in the case of RSM with Sc_t=0.7 the simulations match the experimental results well. The results again reveal high sensitivity of numerical results to variation of Sc_t. Increasing Sc_t towards 0.7 leads to better prediction for both RANS models. The sensitivity of RANS models prediction to variation of Sc_t, are shown in contour form in Figure 11.

The sensitivity of $k-\varepsilon$ results to variation of Sc_t is more evident than for the RSM model. For instance, the $k-\varepsilon$ model with Sc_t=0.2 overpredicts the mixing significantly. Similar to the results of the first plane, use of the RSM turbulence model with Sc_t=0.7 results in best agreement with measured values. In general, the sensitivity of the results to turbulence model appears less than it does in the first plane.

The third plane is located at Z/D=1.875. The radial profiles of predicted fuel to air ratio are shown with the measured values in Figure 12. The numerical results using a Sc_t number of 0.7 provide predictions nearest the measured values. Although the fuel/air profiles predicted by both RANS models with Sc_t of 0.7 vs the experimental data are similar, the peak values differ. Another observation is that the overall mixing level at this plane is greater than at the first plane. For example, the peak magnitude of fuel to air ratio at first plane is about 16 times more than the magnitude of fuel to air ratio at the third plane. It indicates the fast mixing of jet into air due to the surrounding shear layer.

To evaluate the sensitivity of numerical results to variation of Sc_t, Figure 13 presents the qualitative comparison between numerical and experimental measurements.

Note that the sensitivity to Sc_t variation increases with Z location and that the trends in the prediction of fuel to air ratio for both RANS models are consistent. For instance, in both cases, the models with Sc_t=0.2 the numerical prediction suggests near fully mixed conditions which is in contrast to the experimental results. Based on all of the results for methane, it seems apparent that both RANS models provide superior results with standard Sc_t=0.7.

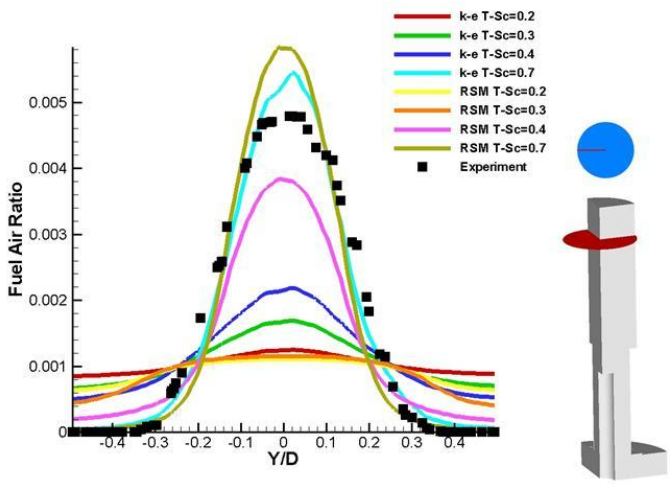

Figure 12- Comparison of measured and predicted methane to air ratio at Z/D=1.875.

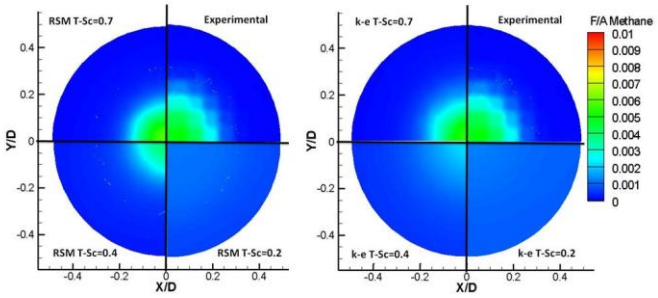

Figure 13- sensitivity of $k-\varepsilon$ and RSM methane to air ratio predictions to various Sc_t at Z/D=1.875.

Thus far, qualitative and quantitative comparisons have been made between numerical and experimental results. The next step in this work is to statistically analyze the results to provide a more comprehensive evaluation. This assessment is made based on the average of the magnitude of fuel air ratio differences between numerical and experimental measurements over the whole plane. The results are normalized by the magnitude of average interpolated experimental measurements for methane air ratio in each plane. The calculated result for methane is given in Figure 14.

Figure 14 summarizes the quality of the CFD predictions at the three planes. The prediction in the first plane is generally the poorest for all of the CFD cases. Also, both $k-\varepsilon$ and RSM models with Sc_t=0.7 have the lowest values which means better agreement with experimental measurement. In general, agreement improves further downstream.

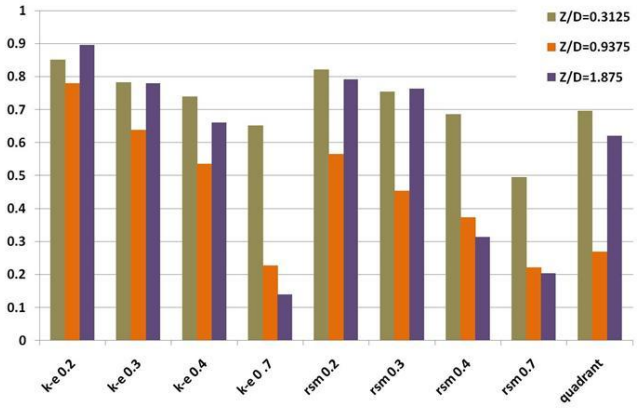

Figure 14- Normalized averaged methane/air differences between experiment and numerical cases.

Hydrogen

In this section, results for the mixing of hydrogen are presented followed by the same organization as used in the part I for methane. It should be noted that, as discussed earlier, the jet momentum ratio for both fuels are set to be similar to facilitate informative comparison. Figure 15 shows the mixing of fuel to air along the centerline. It is observed that the RSM model with Sc_t=0.7 predicts the experimental data closest. It is noted that the laminar Sc for hydrogen and air is 0.2.

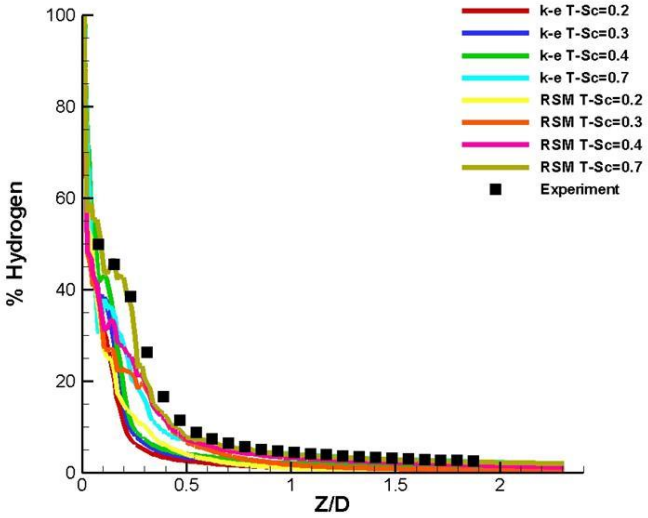

Figure 15- centerline traverse comparison for all of the hydrogen cases at X=Y=0.

The hydrogen to air ratio radial profiles is shown in Figure 16. Note that this first plane is located at Z/D=0.3125, again in the region with highest concentration gradients in the Z direction.

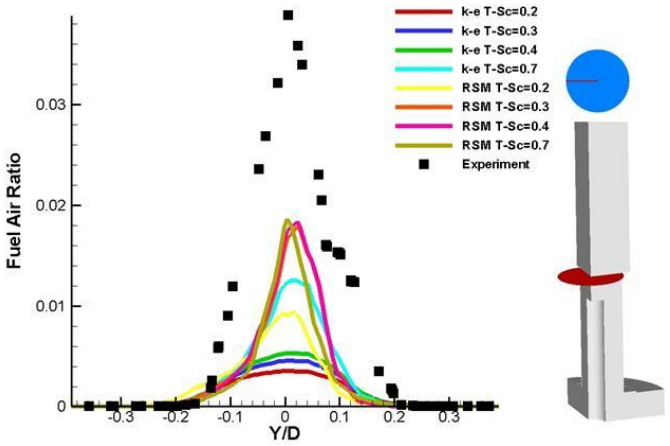

Figure 16- Comparison of measured and predicted hydrogen to air ratio at Z/D=0.3125.

The overall agreement between predicted and measured results is poor. For both turbulence models, the standard Sc_t=0.7 is the best value. However, it is noted that, because this plane is in the region of high axial concentration gradients, small differences in the measurement location vs the prediction location could contribute to the differences observed. While great care is taken to "zero" the probe physical location, even a variation of ~0.5 mm could result in a significant apparent difference.

The sensitivity of predicted values to different Sc_t values is illustrated in the form of contours in Figure 17 for the Z/D = 0.3125 plane.

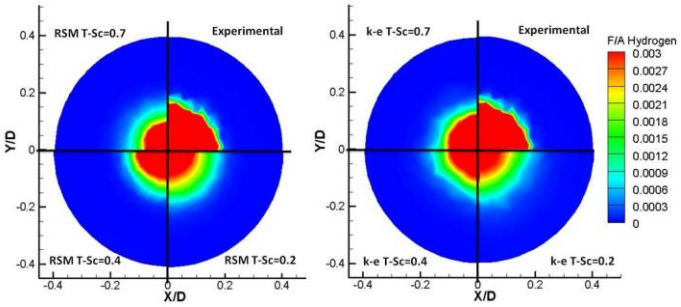

Figure 17- sensitivity of $k-\varepsilon$ and RSM hydrogen to air ratio predictions to various Sc_t at Z/D=0.3125.

In this plane, none of the numerical models can predict the experimental measurements accurately.

The second plane is located at Z/D=0.9375. The radial distribution of hydrogen to air ratio is given in Figure 18. In this plane, the trend of agreement is similar to that observed in the same plane for methane (Figure 10). Both RSM and $k-\varepsilon$ turbulence models with high Sc_t number provide the best agreement with the experimental results. However, as the Sc_t decreases, numerical results overpredict the mixing level as shown in Figure 18 and Figure 19.

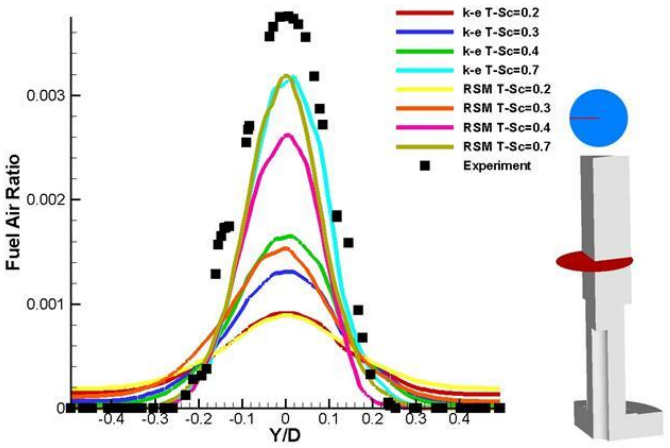

Figure 18- Comparison of measured and predicted hydrogen to air ratio at Z/D=0.9375.

The third plane is located at Z/D=1.875. At this plane RSM and $k-\varepsilon$ turbulence models are able to provide agreement with experimental measurements for high values of Sc_t as shown in Figure 20. However, it is again apparent that selection of appropriate Sc_t is critical. Low Sc_t number leads to misleadingly high levels of mixing.

Contours of fuel to air ratio are presented in Figure 21 to visualize the high sensitivity of numerical results to different Sc_t.

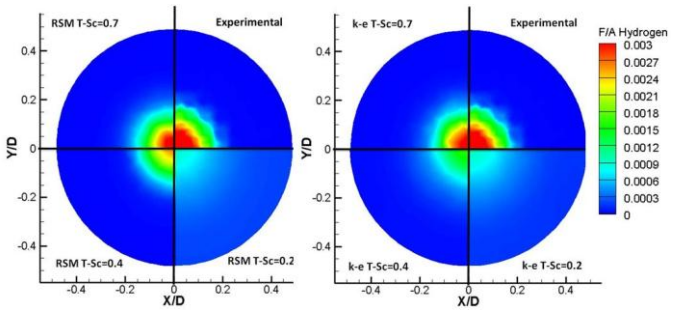

Figure 19- sensitivity of $k-\varepsilon$ and RSM hydrogen to air ratio predictions to various Sc_t at Z/D=0.9375.

In Figure 21 it is apparent that results of RSM and $k-\varepsilon$ models match up well with experimental data. Note again that the overall mixing level at this plane is much higher than at the first plane. The peak magnitude of fuel to air ratio at first plane is about 20 times more than the magnitude of fuel to air ratio at the third plane. Comparing the axial mixing rate to that for methane suggests more rapid mixing for hydrogen.

The statistical analysis of the normalized average difference between the predicted and measured hydrogen/air concentration is presented in Figure 22. These results are consistent with other quantitative and qualitative comparisons in the sense that RSM and $k-\varepsilon$ models with Sc_t=0.7 have the smallest differences.

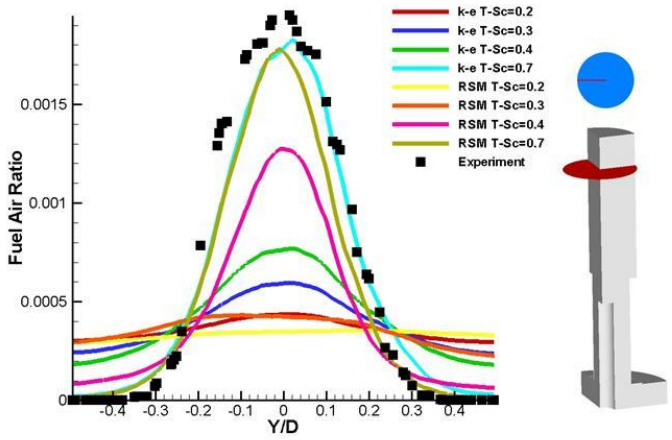

Figure 20- Comparison of measured and predicted hydrogen to air ratio at Z/D=1.875.

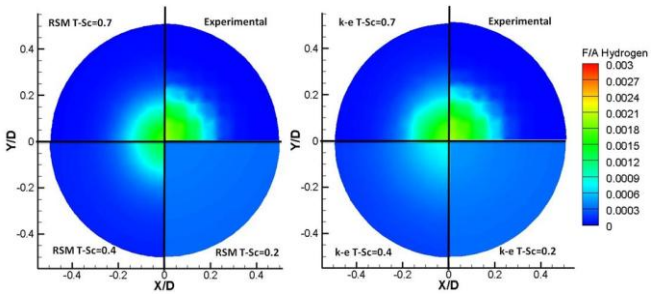

Figure 21- sensitivity of $k-\varepsilon$ and RSM hydrogen to air ratio predictions to various Sc_t at Z/D=1.875.

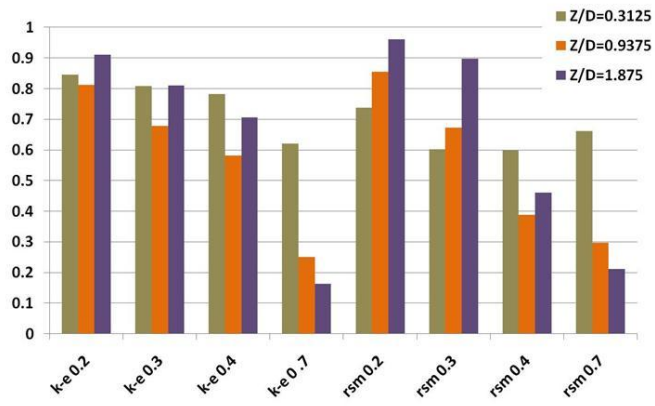

Figure 22- Normalized averaged hydrogen/air differences between experiment and numerical cases.

ANOVA Statistical Results

To further quantify the observations and to explore more subtle guidance, analysis of variance (ANOVA) was carried out for the results. The factors included are 2 fuels, 3 planes, 4 Sc_t numbers, and 2 different RANS models. The response (or performance criteria) is based on the average of the magnitude of fuel air ratio differences between numerical and experimental measurements over the whole plane. It should be noted that the mass flow rates are different for different fuels. Thus, to obtain comparable results for all the cases, the results are normalized by the magnitude of average interpolated experimental measurements for fuel air ratio in each plane. Axial distance is normalized by the main mixing section diameter (D=81.28 mm). Thus, the three planes located at 25.4 mm, 76.2 mm, and 152.4 mm, will be normalized to Z/D=0.3125, 0.9375, and 1.875, respectively.

The result of the ANOVA is summarized in Table 3. As shown, certain individual terms and combination of terms have the greatest effect on the normalized average difference between the predicted and measured fuel concentration. These terms can be used to predict the differences between the measured and predicted fuel/air concentration. A comparison between the modeled difference and actual difference is shown in Figure 23. The good agreement illustrates that the terms with the highest "% Contribution" in Table 3 are essentially responsible for the differences between the measured and predicted fuel/air concentration. As shown, the value of Sc_t is by far the most important factor in attaining good agreement. This is followed by the plane at which the comparison is made. The turbulence model used has some effects and an interaction between the turbulence model used and the value of Sc_t used is noted. It is noticed that the fuel type has little effect.

Table 3-Summary of effects.

Term	SumSqr	% Contribution
A-Turb Model	0.073	2.90*
B-Fuel	0.030	1.21*
C-Plane	0.304	12.13*
D-T-Sch	1.532	61.04*
AB	0.008	0.32
AC	0.002	0.10
AD	0.066	2.61*
BC	0.026	1.05
BD	0.002	0.07
CD	0.353	14.06*
ABC	0.015	0.59
ABD	0.007	0.29
ACD	0.037	1.46
BCD	0.024	0.96
ABCD	0.030	1.21

* Included in response model of normalized average difference, $R^2 = 0.94$

To illustrate how these more important factors affect the agreement, Figure 24 presents a response plot showing how the values of Sc_t and turbulence model selection impact the agreement. As shown, the RSM turbulence model tends to results in better agreement (lower values of $Delta_{LN}$). However, for Sc_t values of 0.7, either turbulence model provides similar agreement. Higher values of Sc_t result in better agreement between predictions and measurements.

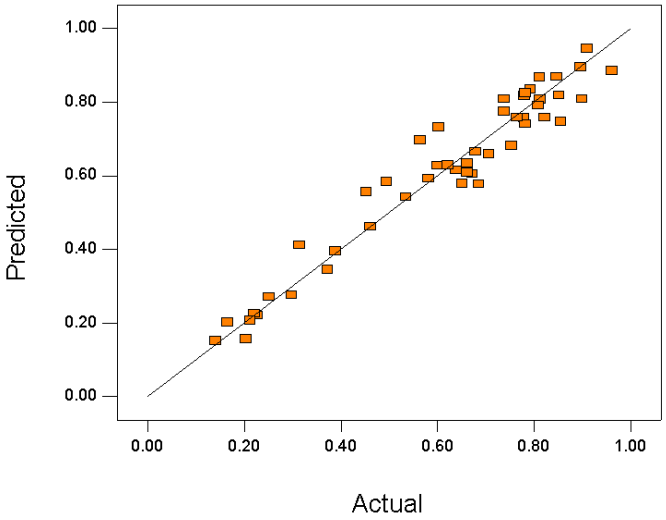

Figure 23- Predicted vs Actual Normalized Average Difference.

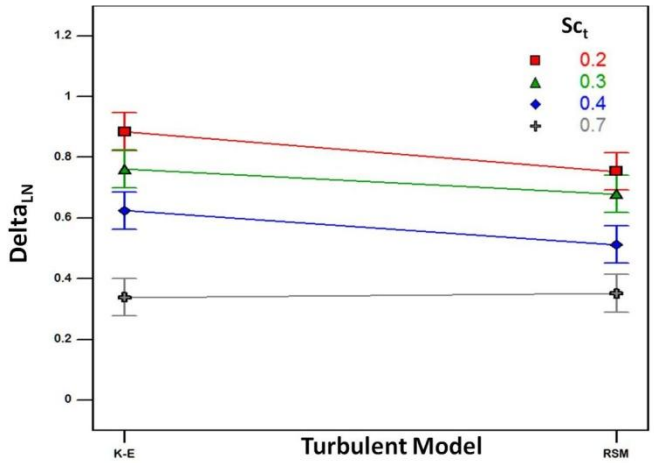

Figure 24- ANOVA analysis for all the RANS axial injection cases.

This statistical analysis is consistent with the qualitative and quantitative comparison in this work. They all demonstrate that RSM and $k-\varepsilon$ models with Sc_t=0.7 provide the most reliable prediction of mass transport flow field in axial injection of fuel into non-swirl co-flow air configuration.

SUMMARY AND CONCLUSIONS

Various RANS simulations were carried out to evaluate the accuracy of different approaches in predicting mixing of methane and hydrogen into a non swirling co-flow of air in a model gas turbine premixer. Comparison of the predictions with local measurement is used as the criteria to evaluate the different numerical approaches. The comparison between numerically predicted and experimentally measured values has been conducted in three different planes downstream of the injection point. Qualitative and quantitative comparison is provided for each plane. Finally, statistical analysis is accomplished for all the studied cases.

The results show that the overall agreement near the injection point is poor. It could be related to sharp change of mass transport properties in this region combined with the accuracy of setting the location for measurements. Planes further downstream have significantly better agreement.

The results for methane and hydrogen are similar. It should be noted that hydrogen and methane are used with similar momentum flux ratio to be comparable. Hydrogen mixing is observed to be faster than methane.

For both fuels, numerical results seem to be sensitive to the selection of appropriate Sc_t. In general, Sc_t=0.7 results in best agreement for this configuration.

The results for both fuels seem to be insensitive to the selection of either $k-\varepsilon$ or RSM turbulent models.

Finally, it is found that, for a matched momentum flux ratio, the dispersion of both methane and hydrogen is very similar; indicating that turbulent shear layer mixing is dominating the jet behavior in the region studied

ACKNOWLEDGMENTS

The support of the U.S. Department of Energy (M. Freeman and R. Dennis) through a University Turbine Systems Research grant is acknowledged.

REFERENCES

[1] J.W.Tester, E.M.Drake, M.J. Driscoll, M.W. Golay, W.A. Peters, 2005, "Sustainable Energy-choosing among options", The MIT Press, Cambridge, Massachusetts.

[2] TN. Veziroglu, F.Barbir, "Hydrogen. The wonder fuel", *International Journal of Hydrogen Energy*. Vol. 17, no. 6, pp. 391-404. 1992

[3] M. Balat , SILA SCIENCE, "Hydrogen in Fueled Systems and the Significance of Hydrogen in Vehicular Transportation", *Energy Sources*, 2007

[4] Richard Derwent, "Global environmental impacts of the hydrogen economy", *Nuclear Hydrogen Production and Application*, 2006

[5] C.Y. TerMaath, E.G. Skolnik, R.W. Schefer, J.O. Keller, "Emissions reduction benefits from hydrogen addition to midsize gas turbine feedstocks", *International journal of Energy*, 2006

[6] J.E. Broadwell and RE Breidenthal, 1984, "Structure and mixing of a transverse jet in incompressible flow", *J Fluid Mech*., Vol 148, pp. 405-412.

[7] A. Akbari, S. Hill, V. McDonell, and S. Samuelsen (2010). Experimental and Computational Analyses of Methane and Hydrogen Mixing in a Model Premixer. Paper GT2010-23049, TurboEXPO 2010, Glasgow, UK, June. to appear, *J. Engr for Gas Turbines and Power*

[8] P.O. Brunn, E. Ryssel, 1998, "Steady non-swirling axisymmetric flows: flow classification and rheological consequences", *Continuum Mechanics and Thermodynamics*, Volume 10, Number 6, 349-357.

[9] D.B. Spalding, 1971, "Concentration fluctuations in a round turbulent free jet", *Chemical Engineering Science*, Volume 26, Issue 1, Pages 95-107.

[10] M. M. Ribeiro, J. H. Whitelaw, 1979, "The Structure of Turbulent Jets", *Proceedings of the Royal Society of London. Series A, Mathematical and Physical Sciences*, Vol. 370, No. 1742 (Mar. 28, 1980), pp. 281-301

[11] F.C. Lockwood, A.S. Naguib, 1975, "The prediction of the fluctuations in the properties of free, round-jet, turbulent, diffusion flames", *Combustion and Flame*, Volume 24, February-June 1975, Pages 109-124.

[12] L.Boguseawski, Cz.O.Popiel, 1978, "Flow structure of the free round turbulent jet in the initial region", *Journal of Fluid Mechanics*, 90 , pp 531-539.

[13] P.O. A. L. Davies, M. J. Fisher, M. J. Barratt, 1962, "The characteristics of the turbulence in the mixing region of a round jet", *Journal of Fluid Mechanics* (1963), 15:3:337-367.

[14] Y. Tominaga, T. Stathopoulos, 2007, "Turbulent Schmidt numbers for CFD analysis with various types of flowfield", *Atm. Env.*, Vol 41, pp. 8091-8099.

[15] J. R. Nanduriab; D. R. Parsonsab; S. L. Yilmazac; I. B. Celikab; P. A. Strakey, 2010, " Assessment Of RANS-Based Turbulent Combustion Models For Prediction Of Emissions From Lean Premixed Combustion Of Methane", *Journal of Combustion Science and Technology*, Volume 182, Issue 7 July 2010 , pages 794 – 821.

[16] S.B Pope, 2000, "Turbulent Flows", Book, Cambridge, New York : Cambridge University Press

[17] FLUENT 6.3 Documentation, "http://my.fit.edu/itresources/manuals/fluent6.3/help/index.htm"

[18] G. BISWAS and S.K. SOM, 1985, "Coefficient of discharge and spray cone angle of a pressure nozzle with combined axial and tangential entry of power-law fluids", *Applied Scientific Research* 43 (1986) 3-22

[19] F. A. Bykovskii and E. F. Vedernikov,1996, "Discharge Coefficients of Nozzles and of Their Combinations in Forward and Reverse Flows", *Journal of Applied Mechanics and Technical Physics*, Vol. 37, No. 4